Journal of Zhejiang University-SCIENCE A (Applied Physics & Engineering)
ISSN 1673-565X (Print); ISSN 1862-1775 (Online)
www.zju.edu.cn/jzus; www.springerlink.com
E-mail: jzus@zju.edu.cn

# Effect of terrain and building structures on the airflow in an airport

Dennis Y. C. LEUNG[†1], W. Y. LO[1], W. Y. CHOW[1], P. W. CHAN[2]

([1]*Department of Mechanical Engineering, The University of Hong Kong, Hong Kong, China*)

([2]*Hong Kong Observatory, Hong Kong, China*)

[†]E-mail: ycleung@hku.hk

Received Oct. 31, 2011; Revision accepted Feb. 13, 2012; Crosschecked Apr. 28, 2012

**Abstract:** The aim of this study was to perform computational fluid dynamics (CFD) simulations on the airflows at the Hong Kong International Airport (HKIA). In particular, the effects of hangar buildings and terrain were studied to explore the effects of turbulence on flying aircraft, especially during landing. The CFD simulation showed that significant differences in wind speeds may occur between the north and the south runways on the western part of the HKIA under typhoon conditions with a strong north to northwesterly wind. Simulation also showed that the hanger buildings between the two runways on the western side and the nearby terrain could be causing the observed difference in the wind speeds. The results also indicated that these obstacles could cause significant wind speed variations at the western end of the south runway. This may affect the operation of landing aircraft. The CFD results for a typical typhoon case were analyzed and found to match the wind data recorded by an aircraft landing that day.

**Key words:** Computational fluid dynamics (CFD), Hong Kong International Airport (HKIA), Low-level wind effect, Hangars, Terrain

**doi:**10.1631/jzus.A1100293 **Document code:** A **CLC number:** O35

## 1 Introduction

With increasing economic development, there has been a steady growth in air traffic all over the world in recent decades. Although many countries are developing high speed trains, air transport is still an indispensable and popular form of transport, particularly for long distance travel. The safety issue is of utmost importance to airline operators. When wind flows over an object, turbulence is usually induced at the rear (wake region) of the object that creates flow disturbances in the surrounding area (Okada and Ha, 1992; Szepesi and Lajos, 1998; Huang *et al.*, 2007). Special attention should be given if this phenomenon happens close to an airport as these airflow disturbances, generated due to the existence of buildings, including navigation towers and hangers, may induce aircraft flight instability which may cause discomfort to passengers and even adversely affect the aircraft operations. In the past decade, many modern international airports have been constructed and commissioned, such as the New Doha International Airport (2012), the Rajiv Gandhi International Airport (2008), the Capital International Airport, Beijing (2008), and the St. George Utah Airport (2007). Due to the forecasted increase in travel demand nationally and internationally, more and more complex buildings have been constructed in modern airports that may induce unwanted flow disturbance to aircraft operations (Neofytou *et al.*, 2006). The extent of disturbance depends on the wind flow characteristics (such as average and gust wind speeds, and turbulence intensity), and nearby building/terrain features (such as the orientation, height and width of buildings/terrain, and their distances from the flight path).

The Hong Kong International Airport (HKIA) is one of the busiest airports in the world. Its geographical location is shown in Fig. 1. Complicated

terrain in Lantau Island (including the mountain Nei Lak Shan, 751 m high) exists at the southern end of the airport, which may lead to wind shear and turbulence when a southerly wind is blowing from the mountain towards the airport. Under a northerly wind blowing from the sea towards the airport, the flow will also be modified by the terrain behind the runways. Chan *et al.* (2010) and Liu *et al.* (2010) found that a low-level wind effect due to artificial structures at the airport, such as terminal buildings and hangars, affects aircraft landing and taking-off on the south and north runways.

There are some cases of suspected building generated low-level wind affecting aircraft operations at the HKIA. For example, on Aug. 23, 2008, under the influence of typhoon Nuri, a strong north-northwesterly wind blew over the HKIA. The anemometers installed at the western ends of the north and the south runways recorded wind speeds of about 19 and 12 m/s, respectively during the period from 10 to 11 am. Two aircraft reported difficulty in landing on the south runway. These difficulties were believed to be due to the strong wind flow disturbance generated by the hangar buildings located close to the runway.

In this study, we investigated the potential effects on airflow of the terrain on the southern side and the hangars on the western side of the HKIA. A computational fluid dynamics (CFD) model was used, which was demonstrated to be able to model the building-induced flow disturbances. A particular focus was a comparison between the simulated north-northwesterly wind flow on the morning of Aug. 23, 2008 and the anemometer readings and available wind data recorded by landing aircraft that day.


**Fig. 1 Geographical setup of HKIA with the complicated terrain on the southern side of the airport**

## 2 Methodology

### 2.1 Computational model

CFD was used to simulate the wind flow, as it is a more economical way to investigate the effect of buildings on wind flow compared with performing physical modeling experiments (Kim and Boysan, 1999; Senthooran *et al.*, 2004; Neofytou *et al*., 2006). In this study, the flow was assumed to be incompressible and the versatile commercial CFD software, FLUENT 6.3.26, was used. A standard *k*-*ε* turbulent model and finite volume method were adopted to solve the continuity (Eq. (1)) and pseudo steady-state momentum conservation (Eq. (2)) equations.

$$\frac{\partial \overline{u}_i}{\partial x_i}=0, \tag{1}$$

$$\overline{u}_j\frac{\partial \overline{u}_i}{\partial x_j}=-\frac{1}{\rho}\frac{\partial \overline{p}}{\partial x_i}-\frac{\partial}{\partial x_j}\overline{u_i''u_j''}, \tag{2}$$

$$\overline{u}_i\frac{\partial k}{\partial x_i}=\frac{\partial}{\partial x_i}\left(\frac{\mu_t}{\rho\sigma_k}\frac{\partial k}{\partial x_i}\right)+\frac{P_k}{\rho}-\varepsilon, \tag{3}$$

$$\overline{u}_i\frac{\partial \varepsilon}{\partial x_i}=\frac{\partial}{\partial x_i}\left(\frac{\mu_t}{\rho\sigma_\varepsilon}\frac{\partial \varepsilon}{\partial x_i}\right)+\frac{1}{\rho}C_{\varepsilon 1}P_k\frac{\varepsilon}{k}-C_{\varepsilon 2}\frac{\varepsilon^2}{k}, \tag{4}$$

where $x_i$ is the Cartesian coordinates; $\overline{u}_i$ is the velocity in the streamwise, spanwise and vertical directions; $p$ is the static pressure; $k$ is the turbulent kinetic energy (TKE); $P_k$ and $\varepsilon$ are the production and dissipation rate of TKE, respectively; $\sigma_k$ and $\sigma_\varepsilon$ are the effective Prandtl numbers for $k$ and $\varepsilon$, respectively; $\rho$ is the fluid density; $\mu_t$ is the turbulent dynamic viscosity; and $C_{\varepsilon 1}$ and $C_{\varepsilon 2}$ are empirical modeling constants.

Both Eqs. (1) and (2) are expressed in tensor notation. The transport equations for TKE (Eq. (3)) and the TKE dissipation rate (Eq. (4)) were solved to close the steady-state Reynolds-averaged Navier-Stokes (RANS) equations. The first-order accurate upwind scheme was used to discretize the above equations while the semi-implicit method for pressure linked equations (SIMPLEs) algorithm was used to solve the implicit pressure-velocity coupling in the incompressible flow. An enhanced wall treatment, consisting of a two-layer model with enhanced wall functions, was used. Higher resolution meshes were set adjacent to the walls to help resolve velocity gradients and turbulent quantities within viscosity-affected

near-wall regions. We expected that the enhanced wall treatment would help resolve the laminar sublayer adjacent to the walls. Details of the mathematical model and its application on a hypothetical terminal building in an airport can be found in (Liu *et al.*, 2010).

Fig. 2 shows the top view of the investigated hangars and associated buildings, which include mainly three Hong Kong Aircraft Engineering Co. Ltd. (HAECO) hangars (hangars 1 to 3) and associated facilities. The buildings investigated are located between the north and south runways.

In general, the maximum power is used for aircraft during take-off, and thus aircraft will be less affected by flow disturbance at take-off than during landing. Therefore, this study focused on the landing operation of aircraft. Major buildings potentially affecting the airflow at the western end of the south runway were included in the CFD simulation, including the HAECO hangars 1 to 3, the China Aircraft Services Ltd. (CASL) hangar and the engineering test-run facility (Fig. 2). The dimensions of the computation domain were 3500 m×3000 m×300 m (length×width×height). These are 20 to 30 times the characteristics length of the building structures under consideration and therefore were considered adequate. About three million grids were assigned for the model and the meshing pattern is shown in Fig. 3. Unstructured meshes were constructed up to 300 m high, which were denser in the first 60 m or so above ground and over the buildings and the runways. A grid independent check was conducted, which indicated that the selected grid size was sufficient. The inlet and outlet airflow directions were generally in line with the prevailing wind direction on the morning of Aug. 23, 2008.

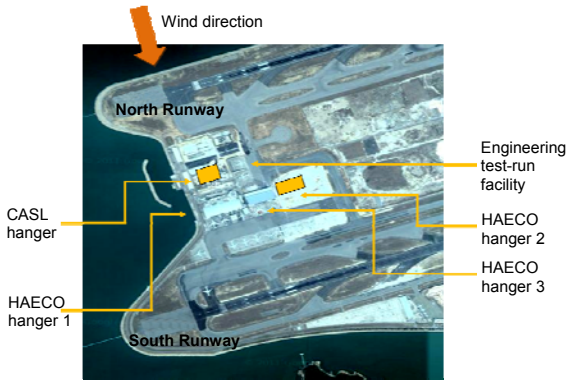


**Fig. 2 Top view of the HKIA with the investigated hangars and associated buildings**

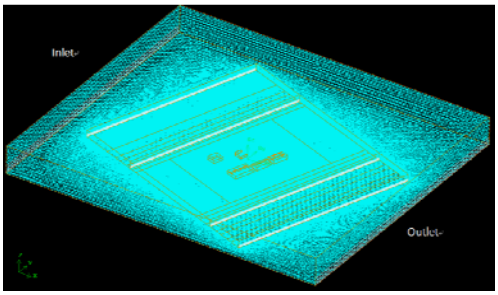


**Fig. 3 Model setup for the simulation on the buildings and runways as well as the meshes assigned in the simulation**

The HKIA was built on reclaimed land with surfaces of different roughness. To make the simulation more realistic, the model adopted different roughness lengths for different surface features (http://www.most.gov.mm/techuni/media/CE_04016_chap5.pdf) as shown in Table 1.

**Table 1 Surface roughness heights adopted for different surfaces**

| Surface type | Roughness height (mm) |
|---|---|
| Sea | 15.2 |
| Concrete | 1.52 |
| Runway | 0.15 |
| Building wall | 1.52 |
| Grass | 15.2 |

## 2.2 Glide path

When an aircraft is going to land, it follows a glide path for the designated runway. Before the touch-down point, it flies towards the runway at an inclined angle of 3°. After touch-down, it moves along the ground and decelerates along the runway. We assumed that the glide path was represented by a line along the centre of the aircraft. Note that the glide path after touch-down was taken to be at a height of 10 m throughout this study.

In this study, both the crosswind (wind blowing from the side of the aircraft) and the headwind (wind blowing towards the head of the aircraft) along the glide path of an aircraft were investigated.

## 2.3 7-knot criterion

A wake region may be formed when wind flows over buildings and structures, causing a deviation in wind speed. A change in headwind will cause a corresponding change in the lift force while a change in

crosswind may cause roll and yaw in the aircraft. According to the wind study report for Amsterdam Airport Schiphol (Krus, 2003), pilots experience difficulties in controlling an aircraft when the crosswind speed drop (the difference between a perturbed and unperturbed wind speed) in the wake region exceeds 7.5 knots (3.6 m/s). Therefore, the "7-knot criterion" was developed so that a warning signal to pilots is given whenever there is a drop in crosswind speed exceeding 7 knots. In this project, the "7-knot criterion" was used to determine whether or not special attention needed to be given to this effect along the glide path of the aircraft.

### 2.4 Wind data

The Hong Kong Observatory has set up several stations to monitor the wind flow close to the airport. In this study the wind profile measured from a radar wind profiler at Sha Lo Wan (Fig. 1) was adopted as the background wind. The wind profiler measured the vertical profile of the horizontal winds (Table 2) but due to the limited model simulation range in the vertical direction, the wind data for only the first two altitudes, 116 m and 174 m, obtained at 10:30 am on Aug. 23, 2008, were used in this study (Table 3). The following is a power law wind profile obtained based on these wind data:

$$u=6.44z^{0.2255}, \tag{5}$$

where $u$ is the wind speed, and $z$ is the altitude above sea level. In the present simulation, a uniform background wind direction of 346° from the north was assumed and used as the inlet flow condition for the model simulation.

## 3 Model validation

Model validation was done by comparing the CFD results with experimental results from previous study. A wind tunnel experiment on a pedestrian wind environment behind buildings was performed by Yoshie *et al.* (2007) to determine the velocity profile around a single building. The experimental model was a rectangular prism with dimensions of 200 mm ×50 mm×200 mm (length×width×height), which was put in a wind tunnel for measurement under a wind speed of 6.7 m/s. In our computation model, the sizes of the building prism and computational domain were the same as in the wind tunnel experiment described above. The streamwise wind profile at the inlet of the wind tunnel was approximated by the power law:

$$\overline{u}=U_{\text{free}}\times\left(\frac{z}{L_z}\right)^{0.27}, \tag{6}$$

where $U_{\text{free}}$ is the free-stream wind speed, and $L_z$ is the vertical extent of the wind tunnel. Fig. 4 shows that the computed normalized streamwise velocities upstream and downstream of the building match well with the experimental measurements. Similar

**Table 2 Background wind profile based on the wind measurement on Aug. 23, 2008 at 10:30 am at the Sha Lo Wan wind profiler**

| Height (m) | Velocity (m/s) | Wind direction (°) |
|---|---|---|
| 116 | 18.8 | 346 |
| 174 | 20.6 | 344 |
| 231 | 20.2 | 347 |
| 289 | 21.4 | 344 |
| 347 | 20.5 | 357 |

**Table 3 Background wind profile for the model simulation after scaling up to match the wind data (at 10 m height) from the runway anemometers at the airport**

| Height (m) | Velocity (m/s) | Wind direction (°) |
|---|---|---|
| 0 | 0 | 346 |
| 10 | 16.7 | 346 |
| 116 | 24.7 | 344 |

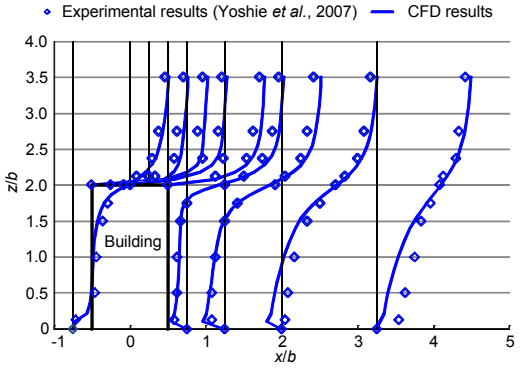


**Fig. 4 Comparison of computed streamwise velocity with experimental results (Yoshie *et al.*, 2007) at different locations in the wake of a building**

$x$ represents the streamwise distance, and $b$ is the building width

agreement was also found for the vertical velocity component. This indicates that the computation model is able to predict the wake velocity accurately.

## 4 Results and discussion

### 4.1 Simulation without buildings/structures and terrain

A simulation without any buildings and terrain was first performed to demonstrate that the presence of the buildings and terrain is the main factor causing flow disturbance on the south runway.

The HKIA airport has installed a number of wind anemometers at different locations to determine the wind environment in the vicinity. Two such sensors were installed at the western ends of the north and south runways and the results of the measurements were used for comparisons with the simulated results (Fig. 5a). The results indicated that similar computed wind profiles exist at these two locations in the absence of any buildings and terrain. Due to the surface roughness, the wind over the south runway is slightly reduced after passing over the ground between the two runways.

Besides the wind at the ground level, the crosswind and headwind speeds along the glide path of the aircraft landing on the south runway were also investigated. Fig. 6a shows that the simulated crosswind speed drops gradually by about 2 m/s along the glide path on the airborne portion and becomes constant after the touch-down point. This drop is due to the drop in wind speed with decreasing altitude in the wind power law.

### 4.2 Simulation with buildings and terrain

The plot of the computed wind profile at the two anemometer points in the presence of the buildings and terrain is given in Fig. 5b. The wind speed at the north anemometer position (upstream of the hangars and mountain) is similar with and without the buildings, while there is a significant reduction in wind speed at the south anemometer position. The reduction is about 4.5 m/s at 10 m height compared to about 1.5 m/s for the previous case without buildings and terrain. This shows that the presence of the buildings and terrain affects the wind characteristics around the area.

Fig. 5c shows the actual measured wind speed at the two anemometer locations during the period from 10 to 11 am on Aug. 23, 2008. Table 4 shows the wind

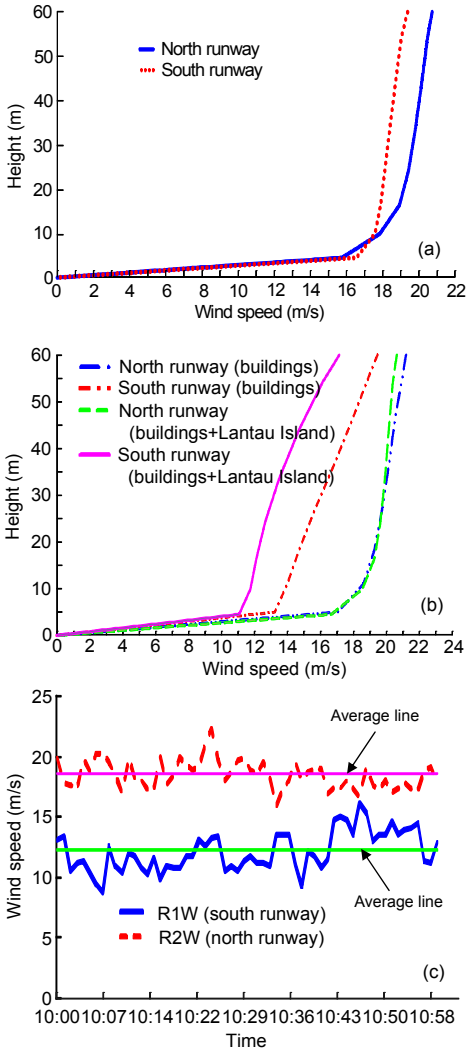


**Fig. 5 Computed wind profiles at the two anemometer locations without buildings and terrain (a), in the presence of buildings and terrain (b), and anemometer readings of R1W and R2W from 10 to 11 am on Aug. 23, 2008 (c)**

**Table 4 Comparison of computed and measured wind speeds on the north and south runways**

| Condition | Wind speed at 10 m height (m/s) | | Difference (m/s) |
|---|---|---|---|
| | North runway | South runway | |
| Without obstacles | 18.5 | 18.0 | 0.5 |
| With building alone | 18.4 | 13.9 | 4.5 |
| With terrain alone | 18.5 | 18.0 | 0.5 |
| With buildings and terrain | 18.5 | 11.8 | 6.7 |
| Actual measurement | 18.5 | 12.1 | 6.4 |

speed at the two anemometer locations under different simulations together with the measured values. The measured and computed differences in wind speed between the two measuring points match well. The readings on the north runway had the same value of 18.5 m/s (fixed for the simulation) while the readings on the south runway had similar values (12.1 and 11.8 m/s, respectively). Comparing the case with and without terrain, we found that the wind speed on the south runway dropped significantly from 13.9 to 11.8 m/s. Therefore, although the terrain is located downwind of both the north and south anemometers, the effect of the terrain cannot be neglected in the computation.

Fig. 7 shows the effect of the wind on the flow-field behind the buildings, and indicates that the wind flow may induce significant effects near the aircraft's touch-down point on the south runway in the presence of the buildings and terrain. This is further illustrated in Fig. 6 which shows the crosswind and headwind along the glide path for a hypothetical landing aircraft moving from the western side of the HKIA towards the south runway without (Fig. 6a) and with (Fig. 6b) the buildings, respectively. There were significant differences in both the crosswind and headwind speeds, particularly for the case with the building structures. In this case (Fig. 6b), the crosswind speed dropped from about 18 m/s at 500 m before the touch-down point to 7 m/s at the touch-down point. The effect continued after touch-down and the wind speed rose rapidly to about 18 m/s at 500 m after the touch-down point. This shows that the building structures obstruct and modify the wind flow near the touch-down point. Further away from the touch-down point, the wind speed generally recovers to its nominal values. The headwind speed also shows a small wind speed fluctuation before and after the touch-down point of the aircraft, but it is insignificant and will not affect aircraft operation.

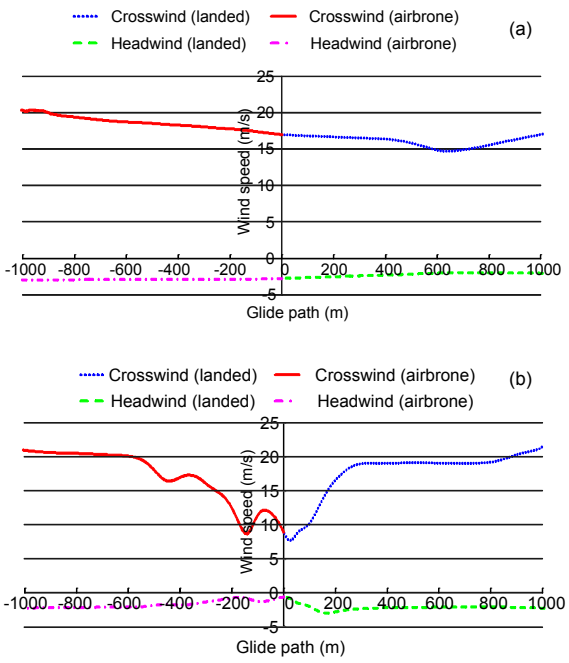


**Fig. 6 Crosswind and headwind speeds along the glide path without buildings (a) and with buildings (b)**

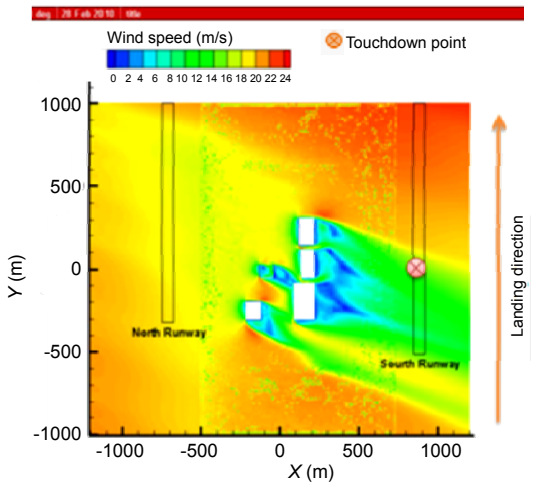


**Fig. 7 Wind speed contours at 10 m above the runway**

### 4.3 Comparison between the CFD results and the pilot report

A pilot report from an aircraft landing at the HKIA on Aug. 23, 2008 was obtained. It reported a strong drop in wind speed at the time of landing. The graphs of the wind profile recorded along the glide path are shown in Fig. 8. There was a rapid drop in crosswind speed starting from 400 m before the touch-down point. A small but insignificant fluctuation in headwind speed along the glide path was observed in both the CFD simulation results and the data from the aircraft.

Fig. 8 also shows that the CFD simulation with buildings and terrain is much better than that without, particularly for the crosswind simulation. Furthermore, a smoother curve is obtained from the onboard aircraft measurements, which could be explained by

the response of the pilot facing sudden drops in wind speed. When an aircraft pilot detects a significant wind speed fluctuation, he/she would respond quickly and correct the flight path immediately. Therefore, a smoother curve is expected to be obtained from the detector onboard the aircraft.

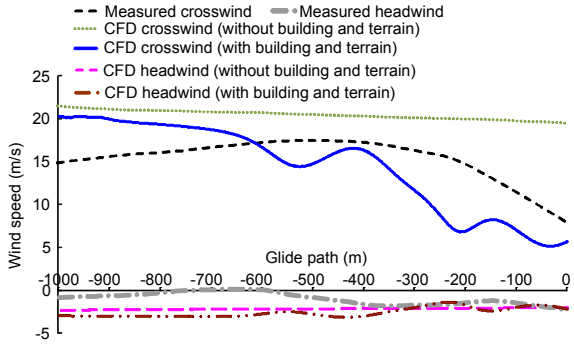


**Fig. 8 Comparison of the wind profiles along the glide path (airborne only) between the pilot report and CFD results**

The upper three lines show the crosswind speed along the glide path while the lower three show the headwind speed

### 4.4 Simulation of the effect of buildings under different wind directions

Further simulations were carried out with different wind directions from 320° to 360° north with an interval of 10°. These are the wind directions under which the building structures considered would have potential effects on the glide path near the touch-down point (Fig. 2). The simulated results show similar profiles as in the previous case but with different degrees of wind speed fluctuations. Table 5 compares the maximum crosswind speed drops within 1 km before landing under different wind directions, and shows that the 7-knot criterion will be exceeded at a wind direction of about 350° (346°–360°) north under the current wind flow situation, and thus the pilot needs to be careful under such conditions.

**Table 5 Comparison of computed maximum crosswind speed drops within 1 km before landing under different wind directions**

| Wind direction (°) | Maximum crosswind speed drop (m/s) | Exceed 7-knot (3.6 m/s) criteria |
|---|---|---|
| 320 | – | No |
| 330 | – | No |
| 340 | 4.4 | Yes |
| 346 | 5.0 | Yes |
| 350 | 5.1 | Yes |
| 360 | 4.6 | Yes |

## 5 Conclusions

The wind flow characteristics at the HKIA were studied using CFD. We found that the presence of buildings and terrain would affect the wind flow in the vicinity of the runways. The wind speed difference between the north and south runways was found to be significantly larger than that when the effects of the buildings and terrain were excluded, which is consistent with the measured anemometer data. The crosswind speed drop along the glide path before the touch-down point was also consistent with a pilot report. A slight headwind speed fluctuation was also noted along the glide path with wind blowing towards the head of the landing aircraft.

The turbulent wakes in different wind directions were also simulated by using a typical typhoon wind profile. We found that the turbulent wake moved from the landed part to the airborne part of the glide path when the simulated wind direction changed from 320° to 360° north. Therefore, it is more difficult for aircraft landing on the south runway when strong wind blows from a direction of about 350° north.

## References

Chan, P.W., Lo, W.Y., Leung, D.Y.C., 2010. Low Level Wind Effects of the Hangars at the Hong Kong International Airport. Proc. 5th International Symposium on Computational Wind Engineering Chapel Hill, North Carolina, USA.

Huang, S.H., Lib, Q.S., Xu, S.L., 2007. Numerical evaluation of wind effects on a tall steel building by CFD. *Journal of Constructional Steel Research*, **63**(5):612-627. [doi:10.1016/j.jcsr.2006.06.033]

Kim, S.E., Boysan, F., 1999. Application of CFD to environmental flows. *Journal of Wind Engineering and Industrial Aerodynamics*, **81**(1-3):145-158. [doi:10.1016/S0167-6105(99)00013-6]

Krus, H.W., 2003. Numerical simulations of wind measurements at Amsterdam Airport Schiphol. *Journal of Wind Engineering and Industrial Aerodynamics*, **91**(10):1215-1223. [doi:10.1016/S0167-6105(03)00079-5]

Liu, C.H., Leung, D.Y.C., Man, A.C.S., Chan, P.W., 2010. CFD simulation of the wind flow over an airport terminal building. *Journal of Zhejiang University-SCIENCE A (Applied Physics & Engineering)*, **11**(6):389-401. [doi:10.1631/jzus.A0900449]

Neofytou, P., Venetsanos, A.G., Vlachogiannis, D., Bartzis, J.G., Scaperdas, A., 2006. CFD simulations of the wind environment around an airport terminal building. *Environmental Modelling & Software*, **21**(4):520-524. [doi:10.1016/j.envsoft.2004.08.011]

Okada, H., Ha, Y.C., 1992. Comparison of wind tunnel and

full-scale pressure measurement tests on the Texas Tech Building. *Journal of Wind Engineering and Industrial Aerodynamics*, **43**(1-3):1601-1612. [doi:10.1016/0167-6105(92)90375-K]

Senthooran, S., Lee, D.D., Parameswaran, S., 2004. A computational model to calculate the flow-induced pressure fluctuations on buildings. *Journal of Wind Engineering and Industrial Aerodynamics*, **92**(13):1131-1145. [doi:10.1016/j.jweia.2004.07.002]

Szepesi, Z.S., Lajos, T., 1998. Wind Tunnel Investigation on Flow and Pollutant Transport Past Two Buildings. Proc. 1st Conference on Mechanical Engineering, Technical University of Budapest, Hungary, p.575-759.

Tsuchiya, M., Murakami, S., Mochida, A., Kondo, K., Ishida, Y., 1997. Development of a new *k*-*ε* model for flow and pressure fields around bluff body. *Journal of Wind Engineering and Industrial Aerodynamics*, **67-68**:169-182. [doi:10.1016/S0167-6105(97)00071-8]

Yoshie, R., Mochida, A., Tominaga, Y., Kataoka, H., Harimoto, K., Nozu, T., Shirasawa, T., 2007. Cooperative project for CFD prediction of pedestrian wind environment in the Architectural Institute of Japan. *Journal of Wind Engineering and Industrial Aerodynamics*, **95**(9-11):1551-1578. [doi:10.1016/j.jweia.2007.02.023]